

## **Predicting tunnel squeezing prior to excavation using machine learning and support pattern**

\*Hyoung-Seok Oh<sup>1)</sup>, Joon-Shik Moon<sup>2)</sup>

*<sup>1), 2)</sup> Department of Civil Engineering, Kyungpook National University, Daegu 41566, Korea*

*<sup>1)</sup> [j.moon@knu.ac.kr](mailto:j.moon@knu.ac.kr)*

### **ABSTRACT**

Tunnel squeezing, a time-dependent deformation phenomenon arising when in-situ stress exceeds rock compressive strength, poses significant challenges for structural stability and operational safety. To predict squeezing prior to tunnel excavation, this study selected parameters for overburden depth (H), tunnel diameter (D), rock mass quality index (Q), Rock Mass Rating (RMR), and the support stiffness (K) that could be obtainable during the design phase. In addition, this study calculated K values based on standard support patterns rather than those previously employed. To predict squeezing, SVM, MLP, Random Forest, and Gradient Boosting models were employed, and data preprocessing was carried out using SMOTE oversampling. The Gradient Boosting model achieved the highest accuracy at 90.48%, followed by Random Forest at 85.71%, Support Vector Machine at 76.19%, and Multilayer Perceptron at 71.43%. Finally, SHAP analysis demonstrated that RMR, D, Q, H, and K, in descending order, exert the influence on squeezing prediction.

### **1. INTRODUCTION**

Deformation caused by squeezing in tunnels can inflict significant damage on the long-term structural stability of tunnels. Squeezing occurs when the stress loading on the rock mass exceeds its uniaxial compressive strength. Aydan et al. (1993) classified the failure modes due to squeezing into three types: (1) complete shear failure accompanied by spalling and sudden slabbing of the surrounding rock, (2) buckling failure occurring in metamorphic or thinly layered ductile sedimentary rocks, and (3) shear and sliding failures commonly observed in thick-bedded sedimentary rocks. Factors contributing to squeezing include tunnel diameter, tunnel shape, overburden depth, lateral pressure coefficient, rock strength, the presence of fault zones, installation of support systems, and tunnel closure. Squeezing in tunnels is a time-dependent deformation phenomenon

---

<sup>1)</sup> Doctoral Candidate

<sup>2)</sup> Professor (Corresponding Author)

that can occur immediately after excavation or develop gradually over several years, leading to construction delays, increased costs, stability issues during construction, and significant maintenance burdens during tunnel operation.

To address these issues, many researchers have attempted to predict squeezing in advance. Methods for predicting squeezing can be broadly classified into geological classification methods, methods based on critical stress and strain, methods based on flow characteristics, and other approaches. Among these, the method proposed by Jethwa et al. (1984), which uses the ground strength constant  $N_c$  calculated as the uniaxial compressive strength divided by unit weight multiplied by overburden depth, is widely used for predicting squeezing. For strain-based methods, the method proposed by Hoek and Marinos (2000), which classifies squeezing into five categories based on the strain  $\varepsilon$  exceeding 1, is commonly used. However, these conventional methods often show reduced accuracy and limitations in advance prediction in fault zones or regions with very high overburden depth.

To overcome these limitations, recent studies have proposed the use of machine learning approaches for squeezing prediction. Table 1. Summarizes previous studies that have utilized machine learning for predicting tunnel squeezing. Jimenez and Recio (2010) predicted squeezing using a linear classification model that classified data based on overburden depth (H) and rock mass quality index (Q). Shafiei et al. (2012) utilized a support vector machine (SVM) model, which finds hyperplanes maximizing the distance between classes in n-dimensional space, to predict squeezing. Subsequently, Huang et al (2021) conducted studies to improve prediction accuracy by combining a backpropagation neural network with SVM models using parameters for tunnel diameter (D) and support stiffness (K), in addition to (H) and (Q). Zhou et al. (2022) further improved prediction accuracy through hyperparameter tuning using the Whale Optimization Algorithm inspired by whale foraging behavior. Sun et al (2018) used a multiclass SVM model to classify squeezing into three stages based on strain: no squeezing when  $\varepsilon < 1$ , minor squeezing when  $1 \leq \varepsilon < 2.5$ , and extreme squeezing when  $\varepsilon \geq 2.5$ . Chen et al. (2020) predicted squeezing in three stages using a decision tree (DT) model. Zhang et al. (2020) conducted research to improve accuracy by ensembling multiple algorithms, including BPNN, SVM, DT, KNN, LR, MLR, and NB. Peng et al. (2025) preprocessed data using the SMOTE technique and predicted squeezing using SVM, RF, DT, XGBoost, LGBM, and KNN models.

To date, these studies have primarily focused on improving the prediction accuracy by enhancing machine learning algorithm models. However, the datasets used in previous studies have typically been constructed by combining additional field data with data collected from various countries. There is insufficient examination of the appropriateness of using the distribution of data collected from different countries as a database for squeezing prediction. Therefore, this study aims to review the appropriateness of the datasets used in previous research and utilize suitable data to predict squeezing using various classification algorithms.

**Table 1** Classification comparison of existing prediction models (Zhou et al. 2022)

Authors	Classifiers	Parameters	Classes
Jimenez & Recio	LC	H, Q	2
Shafiei et al.	SVM	H, Q	2
Sun et al.	M-SVM	H, Q, D, K	3
Chen et al.	DT	H, D, K, SSR, GC	3
Zhang et al.	Ensemble (BPNN, SVM, DT, KNN, LR, MLR, NM)	H, Q, D, K, SSR	2
Huang et al.	SVM-BP	H, Q, D, K	2
Zhou et al.	SVM-WOA	H, Q, D, K, $\epsilon$	2
Peng et al.	SVM, DT, RF, XGBoost, LGB, KNN	H, Q, D, SSR, K	2

## 2. DATA ANALYSIS

This study utilized the open dataset provided by Zhou et al. (2022). In this study, parameters (H), (Q), (D), (RMR) and (K) that can be obtained prior to tunnel construction were selected for analysis. (H) represents the overburden depth of the tunnel, and (Q) and (D) are calculated as shown in Eq. (1) and (2)

$$Q = \left( \frac{RQD}{J_n} \right) * \left( \frac{J_r}{J_a} \right) * \left( \frac{J_w}{SRF} \right) \quad (1)$$

$$D = \sqrt{4A/\pi} \quad (2)$$

( $RQD$  = Rock quality designation,  $J_n$  = joint set number,  $J_r$  = joint roughness number,  $J_a$  = joint alteration number,  $J_w$  = joint water reduction factor,  $SRF$  = stress reduction factor.)

The support stiffness (K) is calculated as the sum of the stiffness of shotcrete, rock bolts, and steel sets, as shown in Equation (3), while the calculation formulas for each are presented in Eq. (4), (5), (6) and (7).

$$K = K_{s(shot)} + K_{s(bol)} + K_{s(set)} \quad (3)$$

$$K_{s(shot)} = \frac{E_{shot}}{(1+\mu_{shot})} \cdot \frac{[a^2 - (a-t_{shot})^2]}{[(1-2\mu_{shot})a^2 + (a-t_{shot})^2]} \cdot \frac{1}{a} \quad (4)$$

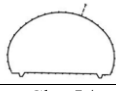
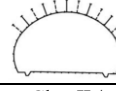
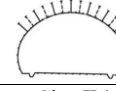
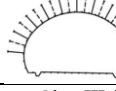



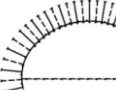
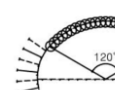
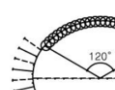
$$K_{s(bol)} = \frac{1}{s_t s_l \left[ \frac{4L_{bol}}{\pi \phi^2 E_{st}} + Q \right]} \quad (5)$$

$$K_{s(set)} = \frac{E_{st} \cdot A_{set}}{d \left[ a - \frac{h_{set}}{2} \right]^2} \quad (6)$$

$$K_{s(set)} = p \frac{a}{u} \quad (7)$$

( $E_{shot}$  = elastic modulus of shotcrete,  $\mu_{shot}$  = Poisson's ratio of shotcrete,  $a$  = radius of tunnel,  $t_{shot}$  = thickness of shotcrete,  $s_t$  = circumferential spacing of rock bolts,  $s_l$  = longitudinal spacing of rock bolts,  $L_{bol}$  = length of rock bolts,  $\phi$  = diameter of rock bolts,  $E_{st}$  = elastic modulus of rock bolts,  $Q$  = a load-displacement constant,  $E_{st}$  = elastic modulus of steel sets,  $A_{set}$  = area of steel sets,  $d$  = distance of steel sets,  $h_{set}$  = height of steel sets,  $p$  = monitored radial support pressure,  $u$  = measured radial deformation)

**Table 2 NATM Tunnel support pattern (Park et al. 2018)**

Classification			TYPE A	TYPE B-1	TYPE B-2	TYPE C-1
Support Pattern Overview						
Rock Mass Classification / Ground Condition			Class I / $RMR \geq 81$	Class II / $80 \geq RMR \geq 71$	Class II / $70 \geq RMR \geq 61$	Class III / $60 \geq RMR \geq 51$
Excavation Method, Advance Length(Crown/Invert), Support length(Crown/Invert)			Fullface, $\geq 4.0m$ , 4.0m	Fullface, 4.0m, 4.0m	Fullface, 3.5m, 3.5m	Fullface, 3.0m, 3.0m
S U P P O R T	Shotcrete	Type, Sealing/Primary/Secondary(mm)	Ordinary, 50/50/-	Steel fiber, 50/50/-	Steel fiber, 50/60/-	Steel fiber, 75/80/-
	Rock Bolt	Length(m), Longitudinal/Transverse Spacing(m)	3.0, Random/Random	3.0, 4.0/2.5	3.0, 3.5/2.0	4.0, 3.0/1.8
	Steel Support	Section, Longitudinal Spacing(m)	-	-	-	-
	Concrete Lining	Type, Thickness(mm)	Unreinforced, 300	Unreinforced, 300	Unreinforced, 300	Unreinforced, 300
Classification			TYPE C-2	TYPE D-1	TYPE D-2	
Support Pattern Overview						
Rock Mass Classification / Ground Condition			Class III / $50 \geq RMR \geq 41$	Class IV / $40 \geq RMR \geq 31$	Class IV / $30 \geq RMR \geq 21$	
Excavation Method, Advance Length(Crown/Invert), Support length(Crown/Invert)			Full face, 2.5m, 2.5m	Full face, 2.0m, 2.0m	Benchcut, 1.5m/3.0m, 1.5m/3.0m	
S U P P O R T	Shotcrete	Type, Sealing/Primary/Secondary(mm)	Steel fiber, 75/90/-	Steel fiber, 100/80/40	Steel fiber, 100/80/40	
	Rock Bolt	Length(m), Longitudinal/Transverse Spacing(m)	4.0, 2.5/1.5	4.0, 2.0/1.5	4.0, 1.5/1.5	
	Steel Support	Section, Longitudinal Spacing(m)	As required (L/G - 50×20×30), 2.5	L/G -50×20×30, 2.0	L/G -50×20×30, 1.5	
	Concrete Lining	Type, Thickness(mm)	Unreinforced, 300	Unreinforced, 300	Reinforced as required, 300	
Classification			TYPE E-1	TYPE E-2	TYPE G-1	
Support Pattern Overview						
Rock Mass Classification / Ground Condition			Class V / $20 \geq RMR \geq 11$	Class V / $RMR \leq 10$	End of NATM excavation	
Excavation Method, Advance Length(Crown/Invert), Support length(Crown/Invert)			Benchcut, 1.2m/2.4m, 1.2m/2.4m	Benchcut, 1.2m/1.2m, 1.2m/1.2m	Benchcut, 1.0m/1.0m, 1.0m/1.0m	
S U P P O R T	Shotcrete	Type, Sealing/Primary/Secondary(mm)	Steel fiber, 100/100/60	Steel fiber, 100/100/60	Steel fiber, 100/100/60	
	Rock Bolt	Length(m), Longitudinal/Transverse Spacing(m)	4.0, 1.5/1.2~1.5	4.0, 1.5/1.5	4.0, 1.0/1.5	
	Steel Support	Section, Longitudinal Spacing(m)	L/G -70×20×30, 1.2	H -100×100×6×8, 1.2	H -100×100×6×8, 1.0	
	Concrete Lining	Type, Thickness(mm)	Reinforced, 300	Reinforced, 300	Reinforced, 300	

**Table 3** Material properties used for support system

TYPE	$E_{shot}$ (MPa)	$E_{st}$ (MPa)	$\mu_{shot}$	$\phi$ (m)	$Q$ (m/MN)
A~B-2	15,000	210,000	0.2	0.022	0.042
C-1~G-1	15,000	210,000	0.2	0.025	0.143

In this paper, the support stiffness  $K$  were calculated with Eq.3 and compared against open-source data. Table 2 shows the Ex-TM standard support patterns for tunnel construction proposed by the Korea Expressway Corporation, while Table 3 lists the material properties used for support system.

**Table 4** Performance of different classifiers at many problems in minor change (Zhou et al. 2022)

Tunnel	Rock type	H(m)	Q	D(m)	K(MPa)
Chameliya hydroelectric project	Talcose phyllite	210.8	0.01	5.4	1575.72
Maneri stage tunnel	Sheared metabasics	450	0.31	5.8	5.1
Chenani-Nashri escape tunnel	Siltstone, silty claystone	733	2.903	6.0	6.25
Maneri-Bhali hydroproject	Fractured quartzite	225	3.6	4.8	1000

**Table 5** Support stiffness for each support pattern

TYPE	K(MPa/m)	TYPE	K(MPa/m)
A	63.45	D-1	157.39
B-1	64.70	D-2	162.48
B-2	71.69	E-1	202.74
C-1	100.17	E-2	202.86
C-2	117.93	G-1	210.22

Table 4, which forms part of the open dataset, lists  $K$  values for tunnels with diameters between 4.8 m and 6 m. A tunnel with an overburden of 225 m,  $Q$  value = 3.6, and tunnel diameter = 4.8 m records  $K=1000$  MPa, whereas another tunnel with an overburden of 450 m,  $Q$ -value = 0.31, and tunnel diameter = 5.8 m shows  $K=5.1$  MPa despite poorer rock conditions. These different come from using different Equation to calculate the steel sets stiffness  $K_{s(set)}$ . Eq. 6 assesses  $K_{s(set)}$  from the distance of steel sets, height of steel sets and elastic modulus of steel sets that measured before excavation, whereas Eq. 7 assesses  $K_{s(set)}$  from the monitored radial support pressure and measured radial displacement that measured after excavation. Consequently, to predict tunnel squeezing prior to excavation, this study recalculated the  $K$  values with Equation 6. Table 5 presents the  $K$  values for the Ex-TM support patterns in a 5 m-diameter tunnel. The calculated range extends from 63.42 MPa/m for type A to 210.22 MPa/m for type G-1. In this study, the analysis employs the Ex-TM  $K$  values assigned to each support pattern according to the corresponding RMR rating.

### 3. PREDICTION MODELS

#### 3.1 Synthetic Minority Over-sampling Technique (SMOTE)

Severe class imbalance skews the empirical distribution toward majority-class regions, causing decision boundaries to underrepresent minority instances. Let the feature space be  $X \subset \mathbb{R}^d$ . For any minority sample  $x_i \in X$ , its set of  $k$  nearest minority neighbors is  $N_k(x_i) = \{x_{i,(1)}, \dots, x_{i,(k)}\}$ , where  $k \in \mathbb{N}$  denotes the neighbor count. Eq.8 indicates that SMOTE chooses one neighbor  $x_{i,(k)}$  uniformly from this set and creates a synthetic point where  $\lambda \in [0, 1]$  is the interpolation coefficient.

$$\tilde{x} = x_i + \lambda (x_{i,(k)} - x_i), \quad \lambda \sim U(0, 1) \quad (8)$$

Because  $\tilde{x}$  lies on the line segment joining the two real observations, the synthetic instance remains inside the local convex hull, thereby expanding minority density without inventing out-of-manifold artefacts and pushing the empirical-risk gradient  $\nabla \hat{R}$  toward the minority side.

The variables  $k$  and  $\lambda$  jointly control synthesis aggressiveness. A small  $k$  tightens synthesis around high-density cores, preserving cluster compactness but risking sensitivity to noise; a large  $k$  blends distant neighbors, smoothing the frontier while potentially obscuring hidden submodes. The coefficient  $\lambda$  determines where the synthetic point falls: values near 0 emphasize the cluster interior (increasing precision), whereas values near 1 favor the cluster boundary (increasing recall). A uniform  $\lambda$  distributes samples evenly; alternative distributions (e.g., Beta(2,5)) can bias synthesis toward the frontier when minority recall is paramount.

#### 3.2 Support Vector Machine

Support Vector Machine (SVM) maximises the margin between classes as described in Eq. (9). The soft-margin formulation is compactly written in Eq. (10) without explicit optimisation keywords. The Gaussian RBF kernel employed is stated in Eq. (11), and Platt scaling for probability calibration appears in Eq. (12).

$$f(x) = w^T \varphi(x) + b = 0 \quad (9)$$

$$\frac{1}{2} \|w\|^2 + C \sum \xi_i, \quad y_i (w^T \varphi(x_i) + b) \geq 1 - \xi_i, \quad \xi_i \geq 0 \quad (10)$$

$$K(x_p, x_q) = \exp(-\gamma \|x_p - x_q\|^2) \quad (11)$$

$$P(y = 1 | f(x)) = 1 / (1 + \exp(Af(x) + B)) \quad (12)$$

Eq. (9) defines the separating hyperplane in feature space. Eq. (10) shows the soft-margin objective and its constraints in a single block, where  $C$  governs the trade-off between margin width and empirical error. Eq. (11) gives the RBF kernel with bandwidth  $\gamma$ , and Eq. (12) converts decision scores into calibrated probabilities.



### 3.3 Gradient Boosting

Gradient Boosting is an ensemble technique that sequentially combines weak learners, typically shallow decision trees, to build a powerful predictive model. The process begins by initializing the model with a constant function  $F_0(x)$  that minimizes the loss function  $L$ . At each iteration  $m$ , pseudo-residuals for each sample  $r_i$  are computed as Eq. (13)

$$r_{im} = - \left. \frac{\partial L(y_i, F(x_i))}{\partial F(x_i)} \right|_{F=F_{m-1}} \quad (13)$$

A new decision tree  $h_m(x)$  is trained to predict these residuals, and the model is updated using a line search to find the optimal coefficient  $\gamma_m$  using Eq. (14)

$$F_m(x) = F_{m-1}(x) + \gamma_m h_m(x) \quad (14)$$

This procedure is mathematically equivalent to performing gradient descent in function space and is based on Friedman's Gradient Boosting Machine (Friedman, 2001). Mathematically, Gradient Boosting optimizes the loss function by iteratively adding weak learners that approximate the negative gradient of the loss. After computing the pseudo-residuals, the new tree's predictions are scaled by  $\gamma_m$ , determined by Eq. (15)

$$F_{m+1}(x) = F_{m-1}(x) + \gamma_m h_m(x), \quad \gamma_m = \arg \min_{\gamma} \sum_{i=1}^n L(y_i, F_m(x_i) + \gamma h_m(x_i)) \quad (15)$$

### 3.4 Random Forest

Random forest, as formalized by Breiman (2001), is an ensemble learning method that constructs a multitude of decision trees using independent bootstrap samples drawn with replacement from the original dataset; final predictions are obtained via majority voting for classification or averaging for regression. The algorithm guarantees asymptotic convergence of the generalization error as the number of trees  $M$  grows without bound, thereby mitigating the overfitting tendencies of single decision trees and ensuring stability in large ensembles (Breiman, 2001).

Training proceeds by combining bootstrap aggregating bagging which generates  $M$  bootstrap replicas of the training set with the random subspace method, whereby at each split a random subset of features ( $\sqrt{p}$  features for classification, where  $p$  is the total number of predictors) is considered. This dual randomness sampling observations and features decorrelates individual trees, leading to substantial variance reduction in the aggregate model without increasing bias (Ho, 1998; Breiman, 2001).

The random forest framework offers robust handling of high-dimensional data without requiring prior feature scaling or distributional assumptions, intrinsic estimation of out-of-bag error for unbiased performance assessment, and measures of variable importance to identify key predictors. However, training and evaluating hundreds or thousands of deep trees incurs significant computational and memory demands, and the ensemble's complexity reduces interpretability relative to individual decision trees (Hastie et al., 2009).

### *3.5 Multi-Layer Perceptron*

Multilayer perceptron (MLP) is a feedforward artificial neural network architecture comprising an input layer, one or more hidden layers of nonlinear neurons, and an output layer. Each neuron computes a weighted sum of its inputs plus a bias term and applies a nonlinear activation function (e.g., sigmoid, ReLU) to produce its output, enabling the modeling of complex, nonlinearly separable patterns.

In the training phase, MLPs minimize a differentiable loss function (such as cross-entropy for classification or mean squared error for regression) via backpropagation paired with gradient-based optimization algorithms (e.g., stochastic gradient descent, Adam). During each iteration, the error gradient is propagated backward through the network to adjust weights and biases, and hyperparameters such as learning rate, mini-batch size, and initialization schemes critically influence convergence and generalization performance.

By virtue of the universal approximation theorem, an MLP with a single hidden layer of sufficient width can approximate any continuous function on a compact domain. MLPs are well-suited for tabular data tasks but can exhibit vanishing or exploding gradient issues in deeper architectures, which necessitates the use of regularization techniques (e.g., dropout, weight decay) and advanced activation functions. Furthermore, for spatial data such as images or sequences, convolutional or recurrent architectures often demonstrate superior efficiency and representational power.

### *3.6 Shapley Additive exPlanations*

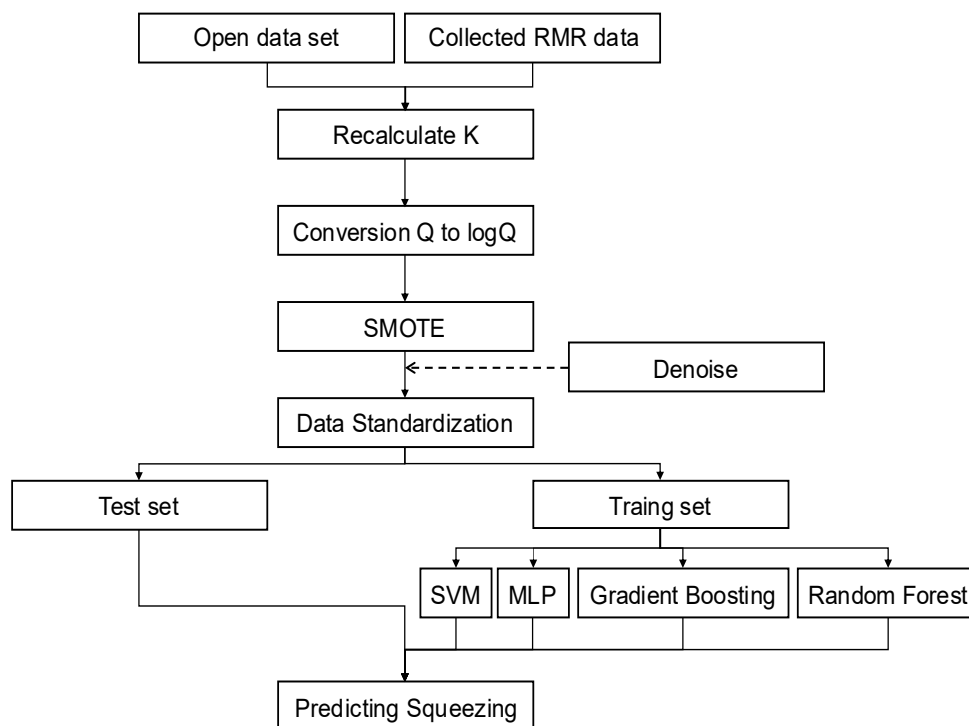
SHAP (Shapley Additive exPlanations) is a model interpretation framework introduced by Lundberg and Lee (2017) that leverages Shapley values from cooperative game theory to quantify each feature's contribution to individual predictions. SHAP uniquely satisfies the properties of consistency, local accuracy, and missingness among additive feature attribution methods, providing a unified explanation framework.

Despite the combinatorial complexity of exact Shapley value computation, SHAP addresses computational challenges through Kernel SHAP an agnostic approximation method using weighted linear regression and TreeSHAP, an exact polynomial-time algorithm optimized for tree ensemble models including XGBoost, LightGBM, CatBoost, and scikit-learn's RandomForest and GradientBoosting implementations.

SHAP supports both local explanations of individual predictions and global insights such as feature importance rankings, interaction values, summary plots, dependence plots, and clustering visualizations, greatly enhancing model interpretability.

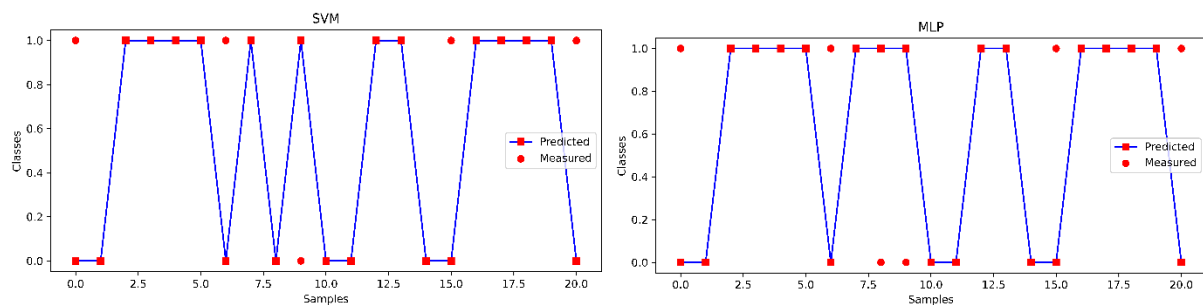


#### 4. SQUEEZING PREDICTION



**Fig. 1** Flowchart for Squeezing Prediction

The sequence of procedures for this study is illustrated in Fig.1. First, RMR data were gathered literature review and open datasets assembled into the study dataset. Next, as described in Chapter 2, the K values were converted to correspond with the support pattern, and log Q was used as a parameter instead of raw Q because 84.75 % of the Q values were below 1, 14.41 % ranged from 1 to less than 20, and only 0.84 % were 20 or higher. Then, to address the imbalance between classes with and without squeezing occurrence, oversampling was performed using the SMOTE technique while simultaneously removing outliers. Finally, the data were split into test and training sets at a 2:8 ratio, and squeezing was predicted using SVM, MLP, Random Forest, and Gradient Boosting models.



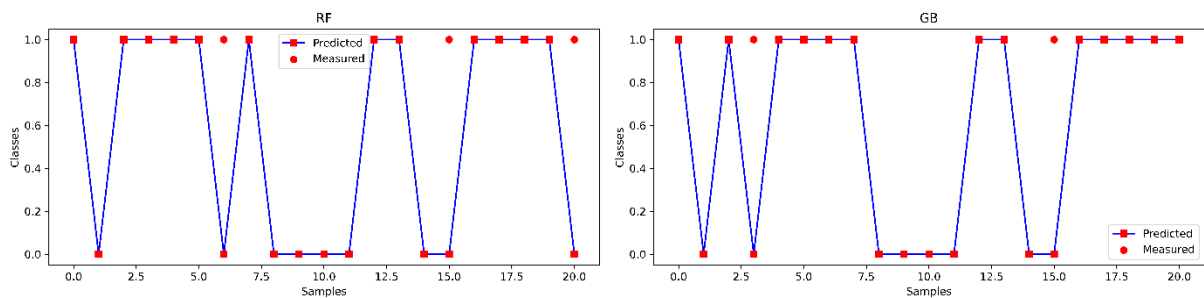


Fig. 2 Predicted classification results on test datasets

Table 6 Performance of different predicting models

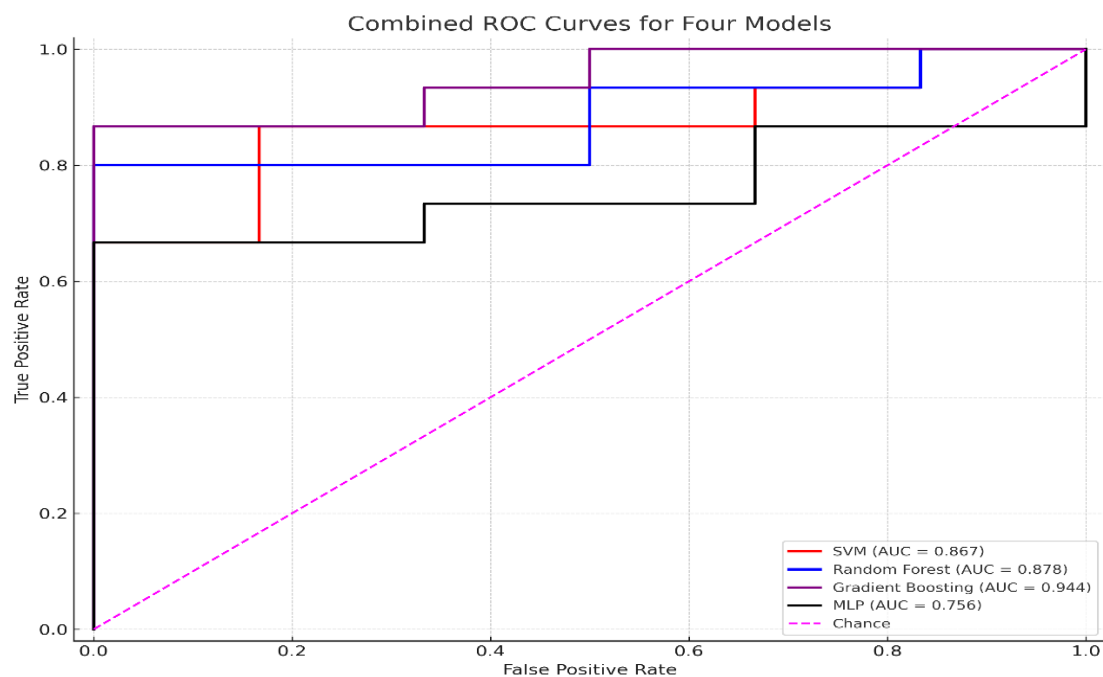
	Precision	Recall	F1-score	Precision	Recall	F1-score
SVM				MLP		
Non-Squeezing	0.56	0.83	0.67	0.5	0.67	0.57
Squeezing	0.92	0.73	0.81	0.85	0.73	0.79
Total Accuracy			0.7619			0.7143
RF				GB		
Non-Squeezing	0.67	1	0.8	0.75	1.0	0.86
Squeezing	1	0.8	0.89	1	0.87	0.93
Total Accuracy			0.8571			0.9048

Figure 2 visually corroborates these findings by plotting predicted versus measured classes across 21 test samples. SVM and MLP traces exhibit frequent deviations visible as crossovers between red dots (measured) and blue squares (predicted) highlighting inconsistent classification in transitional samples. In contrast, RF and GB traces closely track the ground truth, with only isolated misclassifications. GB, in particular, shows minimal divergence, underlining its superior generalization and robustness to class imbalance and feature nonlinearity.

Table 6 summarizes the performance metrics of four classification models Support Vector Machine (SVM), Multilayer Perceptron (MLP), Random Forest (RF), and Gradient Boosting (GB) applied to predict tunnel squeezing events based on D, H, log Q, RMR, K features. The overall accuracy increases sequentially: SVM 76.19%, MLP 71.43%, RF 85.71%, and GB 90.48%. Notably, tree-based ensemble methods outperform the linear and neural classifiers, with GB achieving the highest precision, recall, and F1 scores for both non-squeezing and squeezing classes.

Quantitatively, SVM attains high precision 0.92 for the squeezing class but at the expense of lower recall 0.73, indicating some false negatives. Conversely, its non-squeezing recall is strong 0.83 but with modest precision 0.56, suggesting false positives. MLP yields balanced but lower F1-scores 0.57 non-squeezing, 0.79 squeezing, reflecting its limited capacity to separate overlapping class distributions in the given feature space.

RF demonstrates substantial improvement: non-squeezing precision and recall both reach or exceed 0.80, and squeezing recall is 0.80 with perfect precision 1.00, resulting in an overall F1 of 0.89 for squeezing and 0.80 for non-squeezing. GB further refines this balance, producing recall values of 1.00 non-squeezing and 0.87 squeezing with high precision 0.75 and 1.00 respectively, yielding F1-scores of 0.86 and 0.93 and elevating total accuracy to over 90%.

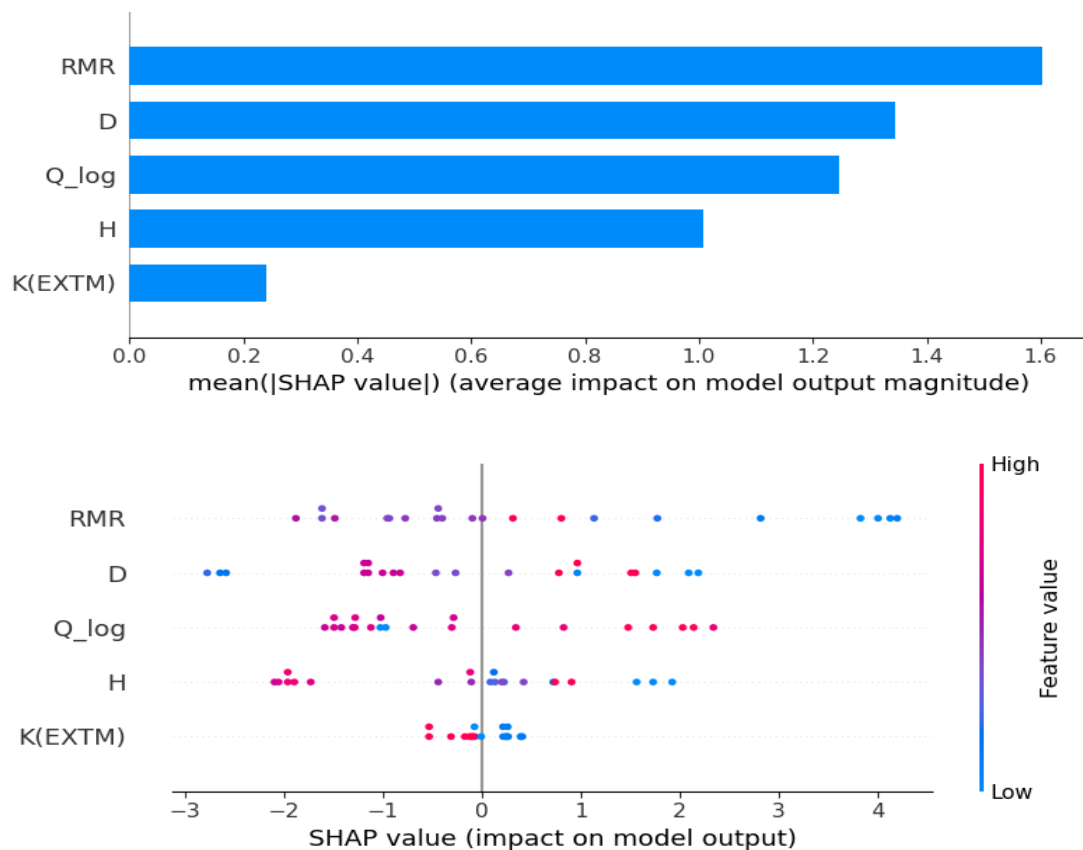


**Fig. 3** ROC curves for four Models

Fig. 3 shows the combined ROC curves for four classification models SVM, RF, GB, and MLP evaluated on the same test set. The corresponding AUC values are SVM = 0.867, RF = 0.878, GB = 0.944, and MLP = 0.756.

The ROC curve illustrates the trade-off between True Positive Rate sensitivity and False Positive Rate ( $1 - \text{specificity}$ ) across all possible decision thresholds. A model with an AUC closer to 1.0 achieves better discrimination between the positive and negative classes. In this comparison, Gradient Boosting demonstrates the highest discriminative power AUC = 0.944, followed by Random Forest AUC = 0.878, and SVM AUC = 0.867. The MLP lagged with the lowest AUC 0.756, indicating weaker overall predictive performance.

Gradient Boosting's ROC curve shows a rapid ascent to high True Positive Rates with minimal increase in False Positive Rate, reflecting strong performance even at low false-alarm levels. Random Forest follows a similar, albeit slightly less pronounced, pattern. SVM achieves a reasonable balance but may benefit from further tuning of its kernel and regularization parameters. The MLP curve is relatively flatter, suggesting that its current architecture and hyperparameters may not capture the underlying class separation as effectively.



**Fig. 4** Results of Parameter importance analysis using SHAP

Figure 4 presents the results of parameter-wise importance analysis performed using SHAP on the Gradient Boosting model trained to predict tunnel squeezing. The top panel shows the SHAP summary dot plot, where each point represents a single test sample's SHAP value for a given feature, colored by the feature's value blue for low, red for high. The bottom panel displays the mean absolute SHAP values as a bar chart, indicating the average impact of each feature on the model's output magnitude.

The ranking of feature importance by mean  $|\text{SHAP value}|$  is RMR 1.68, D 1.36,  $\log(Q)$  1.27, H 1.03, and K(Ex-TM) 0.28. Thus, rock mass rating RMR is the most influential predictor, followed by tunnel diameter D and the rock mass quality index  $\log(Q)$ . Excavation depth H also contributes substantially, while the reinforcement stiffness coefficient K(EXTM) has the least impact under the current dataset and model configuration.

In the summary dot plot, higher RMR values (red points) shift the SHAP values positively, indicating that stronger rock masses increase the probability of non-squeezing classification. Conversely, low RMR (blue points) leads to negative SHAP contributions and a higher likelihood of squeezing. A similar trend is observed for D; larger diameters tend to increase SHAP values, aligning with the understanding that larger diameters are more prone to deformation and thus require higher classification probabilities for squeezing, depending on other covariates.

The excavation depth  $H$  shows a moderate positive influence when deep red samples, suggesting deeper cover increases the risk of squeezing, consistent with geomechanical theory. The relatively low importance of  $K(\text{Ex-TM})$  suggests that, within the range of support patterns considered, variations in reinforcement stiffness play a secondary role compared to ground properties, tunnel diameter and tunnel height.

Additionally, the lower importance of the  $K$  value compared to previous studies can be attributed to the fact that, unlike open datasets where the distribution of  $K$  values varied drastically depending on the calculation method, the distribution of  $K$  values based on support patterns is relatively narrow, resulting in a reduced impact on model predictions.

## **5. CONCLUSION**

This study has demonstrated the effectiveness of machine learning in predicting tunnel squeezing using open dataset. In this study, unlike previous studies, we computed the  $K$  values according to support patterns and incorporated them into the dataset. By leveraging four distinct classification models (SVM, MLP, RF, and GB) and incorporating targeted data preprocessing steps, the research achieved a comprehensive performance comparison under consistent testing conditions. The GB model emerged as the superior predictor, achieving an accuracy of 90.48%, an AUC of 0.944, and balanced precision and recall across both squeezing and non-squeezing classes.

Key findings from SHAP-based interpretability analysis revealed that RMR exerts the greatest influence on model outputs, followed by tunnel diameter, rock mass quality index (log-transformed), and excavation depth. The support stiffness coefficient  $K$  exhibited a relatively narrow distribution range under the adopted Ex-TM support patterns and thus contributed minimally to predictive performance in this context.

The superior performance of ensemble tree methods underscores their ability to capture complex, non-linear relationships among input variables and to diminish overfitting through averaging of weak learners. Gradient Boosting, in particular, showed notable resilience to class imbalance and sensitivity to critical geotechnical features, making it a robust choice for operational forecasting of squeezing. SVM and MLP models, while capable of reasonable discrimination, displayed limitations in handling intricate feature interactions without extensive kernel or architecture tuning.

From an engineering perspective, the results validate the integration of data-driven predictive analytics into tunnel design and monitoring workflows. Accurate prediction of squeezing risk enables proactive support design adjustments, optimizing resource allocation and enhancing safety.

This work also highlights several avenues for future research. First, expanding the dataset with site-specific monitoring records, including time-series deformation measurements and loads borne by support system, could enhance model generalizability. Second, in addition to predicting squeezing, research should also be conducted on developing reinforcement measures at sites where squeezing has occurred. If squeezing is predicted using a sufficiently large and reliable dataset, and appropriate reinforcement measures are determined accordingly, engineers will be able to resolve the stability and economic issues caused by squeezing during tunnel construction and thus carry out more reliable designs.

## REFERENCES

- Aydan, Ö., Akagi, T., & Kawamoto, T. (1993). "The squeezing potential of rocks around tunnels; theory and prediction", *Rock mechanics and rock engineering*, **26**(2), 137-163.
- Jethwa, J. L., Singh, B., & Singh, B. (1984). "28 estimation of ultimate rock pressure for tunnel linings under squeezing rock conditions—a new approach", In *Design and Performance of Underground Excavations: ISRM Symposium—Cambridge, UK, 3–6 September 1984* (pp. 231-238). Thomas Telford Publishing.
- Hoek, E., & Marinos, P. (2000). "Predicting tunnel squeezing problems in weak heterogeneous rock masses", *Tunnels and tunnelling international*, **32**(11), 45-51.
- Jimenez, R., & Recio, D. (2011). "A linear classifier for probabilistic prediction of squeezing conditions in Himalayan tunnels". *Engineering geology*, **121**(3-4), 101-109.
- Shafiei, A., Parsaei, H., & Dusseault, M. B. (2012). "Rock squeezing prediction by a support vector machine classifier", In *ARMA US Rock Mechanics/Geomechanics Symposium* (pp. ARMA-2012). ARMA.
- Huang, Z., Liao, M., Zhang, H., Zhang, J., Ma, S., & Zhu, Q. (2022). "Predicting tunnel squeezing using the SVM-BP combination model", *Geotechnical and Geological Engineering*, **40**(3), 1387-1405.
- Zhou, J., Zhu, S., Qiu, Y., Armaghani, D. D., Zhou, A., & Yong, W. (2022) "Predicting tunnel squeezing using support vector machine optimized by whale optimization algorithm", *Acta Geotechnica*, **17**(4), 1343-1366.
- Zhang, J., Li, D., & Wang, Y. (2020). "Predicting tunnel squeezing using a hybrid classifier ensemble with incomplete data", *Bulletin of Engineering Geology and the Environment*, **79**(6), 3245-3256.
- Sun, Y., Feng, X., & Yang, L. (2018). "Predicting tunnel squeezing using multiclass support vector machines", *Advances in Civil Engineering*, **2018**(1), 4543984.
- Guan, P., Ou, G., Liang, F., Luo, W., Wang, Q., Pei, C., & Che, X. (2025). "Tunnel squeezing prediction based on partially missing dataset and optimized machine learning models", *Frontiers in Earth Science*, **13**, 1511413.
- Park, J.Y., Choi, B.U. and Kim, Y.G. (2018), "Comparative Analysis of NATM Tunnel Construction Costs by Construction Categories and Support Patterns: Focusing on Highway Tunnels", *Magazine of Korean Tunnelling and Underground Space Association*, **20**(1), 35-47
- Friedman, J. H. (2001). "Greedy function approximation: a gradient boosting machine", *Annals of statistics*, 1189-1232.
- Breiman, L. (2001). "Random forests", *Machine learning*, **45**(1), 5-32.
- Ho, T. K. (1998). "The random subspace method for constructing decision forests", *IEEE transactions on pattern analysis and machine intelligence*, **20**(8), 832-844.
- Lundberg, S. M., & Lee, S. I. (2017). "A unified approach to interpreting model predictions", *Advances in neural information processing systems*, **30**.
- Sripad, S. K., Raju, G. D., Singh, R., & Khazanchi, R. N. (2007). "Instrumentation of underground excavations at Tala hydroelectric project in Bhutan", In *Proceedings of international workshop on experiences and construction of tala hydroelectric project Bhutan, New Delhi, India* (pp. 269-282).



- Basnet, C. B. (2013). "Evaluation on the Squeezing Phenomenon at the Headrace Tunnel of Chameliya Hydroelectric Project", Nepal (Master's thesis, Institutt for geologi og bergteknikk).
- Kumar, N. (2002). "Rock mass characterization and evaluation of supports for tunnels in Himalaya", *Department of Civil Engineering, Indian Institute of Technology Roorkee, Roorkee, India*.
- Goel, R. K., Jethwa, J. L., & Paithankar, A. G. (1995). "Indian experiences with Q and RMR systems", *Tunnelling and underground space technology*, **10**(1), 97-109.
- Hoek, E. (2001). Big tunnels in bad rock. *Journal of Geotechnical and Geoenvironmental Engineering*, **127**(9), 726-740.
- Goel, R. K., Jethwa, J. L., & Paithankar, A. G. (1995). "Tunnelling through the young Himalayas—a case history of the Maneri-Uttarkashi power tunnel", *Engineering Geology*, **39**(1-2), 31-44.
- Goel, R. K. (1994). "Correlations for predicting support pressures and deformations in tunnels", *Department of Mining Engineering, Visvesvaraya Regional College of Engineering*.
- Choudhari, J. B. (2007). "Closure of underground opening in jointed rocks", *Department of Civil Engineering. Roorkee, Uttarakhand*.
- Dube, A. K. (1979). "Geomechanical evaluation of tunnel stability under failing rock conditions in a Himalayan tunnel", *Department of Civil Engineering, University of Roorkee, Roorkee, India*.
- Authority, N. E. (2002). "Geology and Geotechnical Report, Volume IV-A and Geological Drawings and Exhibits", Volume VC. *Project Completion Report, NE Authority, Kaligandaki "A" Hydroelectric Project, Syanga, Nepal*.
- Panthi, K. K., & Nilsen, B. (2007). "Uncertainty analysis of tunnel squeezing for two tunnel cases from Nepal Himalaya", *International Journal of Rock Mechanics and Mining Sciences*, **44**(1), 67-76.
- Singh, M., Singh, B., & Choudhari, J. (2007). "Critical strain and squeezing of rock mass in tunnels", *Tunnelling and underground space technology*, **22**(3), 343-350.
- Shrestha, G. L. (2006). "Stress induced problems in Himalayan tunnels with special reference to squeezing", *Faculty of Engineering Science and Technology Department of Geology and Mineral Resources Engineering, Doctoral t.*